ELSEVIER

Journal of Hazardous Materials B131 (2006) 103–111

Journal of Hazardous Materials

www.elsevier.com/locate/jhazmat

Adsorption kinetics of Cu(II) ions using *N*,*O*-carboxymethyl-chitosan

Shengling Sun [a,b], Aiqin Wang [a,*]

[a] *Lanzhou Institute of Chemical Physics, Chinese Academy of Sciences, Lanzhou 730000, PR China*
[b] *Graduate School of the Chinese Academy of Sciences, Beijing 100039, PR China*

Received 3 June 2005; received in revised form 3 September 2005; accepted 10 September 2005
Available online 7 December 2005

Abstract

A series of *N*,*O*-carboxymethyl-chitosan (*N*,*O*-CMC) with different degree of substitution (DS) were prepared by using chitosan (CTS) and monochloroacetic acid under various conditions. The adsorption properties of *N*,*O*-CMC were evaluated. The results revealed that *N*,*O*-CMC is suitable for adsorbent to removal Cu(II) ion. The parameters for the adsorption of Cu(II) ions by *N*,*O*-CMC were also determined. It was shown that the samples of *N*,*O*-CMC had given good correlation with Langmuir's isotherm model and that the adsorption kinetics of Cu(II) could be best described by the pseudo-second-order model. It was also observed that the adsorption capacity seemed to be dependent on pH value in solution, the DS of samples and ionic strength. Furthermore, the maximum adsorption capacity of the monolayer was 162.5 mg of Cu(II) per gram of polymer with DS of 0.96. FTIR and X-ray photoelectron spectroscopy revealed that Cu(II) ions and *N*,*O*-CMC formed a chelate complex.

Keywords: Synthesis; Adsorption; Carboxymethyl-chitosan; Copper ions; Kinetics

1. Introduction

The effluents of industrial wastewaters often contain considerable amounts of toxic and polluting heavy metals. Toxic metals ions in trace quantities are difficult to remove from aqueous solution. Adsorption is the promising alternatives for such situations, especially using low-cost adsorbents like clay material, agricultural wastes and seafood processing wastes. Biosorption or sorption to material of biological origin is recognized as an emerging technique for the treatment of wastewater containing heavy metals [1].

Chitosan (CTS) has been reported for the high potentials of adsorption metal ions [2–7], principally due to the presence of hydroxyl and amine groups that can serve as chelating sites and can be chemically modified in the polymer. The modification of the polymer surface through the introduction of new complexation groups may result in the formation of different chelates, so increasing its adsorption capacity and selectivity toward metal ions in solution [8–10].

Generally, a partial *N*-acetylation or chemical modification is required. Various studies were conducted to make derivatives of CTS by chemical modification techniques, such as PEG-grafting, sulfonation, quaternarization [11], *N*- and *O*-hydroxylation and carboxymethylation-chitosan [12]. Among the derivatives, carboxymethyl-chitosan (CMC) is an amphiprotic ether derivatives, which contains hydroxyl (–OH), carboxyl (–COOH) and amine ($-NH_2$) groups in the molecule, and makes it possible to offer enough chelate groups for increasing adsorption capacity toward metal ions. The adsorption properties of *N*- and *O*-CMC have previously been reported in the literature [13–16]. However, the reports about the adsorption ability of *N*,*O*-CMC for metal ions are scarce, and its adsorption mechanism has not been reported up to now.

Copper may be found as a contaminant in food, especially shellfish, liver, mushrooms, nuts and chocolate. Briefly, any processing or container using copper material may contaminate the product such as food, water or drink [17]. Excessive intake of copper results in an accumulation in the liver. It is also toxic to aquatic organisms even at very small concentrations in natural water.

The aim of this study was to prepare *N*,*O*-CMC and investigate the adsorption ability and the adsorption mechanism of *N*,*O*-CMC toward copper ion in aqueous medium. The influence of various experimental conditions on the adsorption capacity of *N*,*O*-CMC for copper ions such as degree of substitution (DS), pH value and the ionic strength were investigated, and the mech-

* Corresponding author. Tel.: +86 931 4968118; fax: +86 931 8277088.
E-mail address: aqwang@lzb.ac.cn (A. Wang).

0304-3894/$ – see front matter © 2005 Elsevier B.V. All rights reserved.
doi:10.1016/j.jhazmat.2005.09.012

anism of Cu(II) adsorption was analyzed by X-ray photoelectron spectroscopy and several kinetic models. This information will be useful for further applications of system design in the treatment of practical waste effluents.

2. Experimental

2.1. Materials

CTS with 40 mesh, 90% degree of deacetylation (DD) and molecular weight of 6×10^5 was used as received. Monochloroacetic acid, ethanol, acetic acid, sodium hydroxide, hydrochloric acid, copper sulfate, ammonium chloride and sodium chloride used in the experiment were of analytical.

2.2. Synthesis of N,O-CMC

N,*O*-CMC was prepared by the method of Chen and Park [18]. CTS (2.00 g) was dipped into a 20 wt.% sodium hydroxide solution (20.00 mL) for 12 h, and separated by filtration. The treated CTS was added to 15.00 mL of anhydrous alcohol in a three-necked flask by stirring for 30 min at room temperature, then monochloroacetic acid (1.43 g), with dissolving in anhydrous alcohol (10.00 mL), was added into the reaction mixture solution and stirred for additional 30 min. Then the flask was placed in oil bath with a certain temperature and heated for a certain time with stirring. Finally, the contents were poured into a 50 mL beaker followed by the addition of acetic acid solution with stirring until pH value equaled 9.5. The precipitate was filtered, washed with ethanol (70%) for three times and anhydrous alcohol once, and then dried under vacuum. The products were sodium salt of *N*,*O*-CMC and the preparation conditions of the samples with different DS are shown in Table 1.

2.3. Measurement of DS

The DS value of each sample was estimated from Potentiometric titration [19,20]. The alkalimetric curves were recorded on a Mettler Toledo 320 pH meter. Dry *N*,*O*-CMC (0.20 g) was dissolved in 20.00 mL of hydrochloric acid standard solution (0.1000 mol/L). Methyl orange indicator was added. A standard solution of sodium hydroxide was used for titration. Sodium hydroxide volume and pH value acted as horizontal coordinates and vertical coordinates, respectively. And the one or two factorial differential coefficient figure could be gained. The mutation point in this figure was sodium hydroxide volume at the end of titration. The following formulas were used to calculate the total DS and the content of dissociative amido of the sample:

$$\text{total DS} = \frac{(V_2 - V_1) \times C \times \text{molar weight of chitosan residue}}{1000W}$$

$$-\text{NH}_2\ (\%) = \frac{(V_3 - V_2) \times C \times \text{molar weight of chitosan residue}}{1000W}$$

molar weight of chitosan residue

= atomic weight of nitrogen/the average nitrogen content

where C is the concentration of sodium hydroxide standard solution (mol/L). V_1 the sodium hydroxide volume for titrating excessive hydrochloric acid (mL), and V_2, V_3 are the volumes corresponding to titration terminal of –COOH and NH_3^+, respectively. W is the weight of the sample (g).

2.4. Adsorption experiments

All batch experiments were performed on a THZ-98A thermostated shaker with a shaking of 120 rpm, and were carried out using *N*,*O*-CMC with DS of 0.96 as adsorbent (except the effect of DS tests).

In the adsorption equilibrium experiments, 0.10 g of *N*,*O*-CMC and 25.00 mL of sulfate solution buffered at pH 5.0 containing several concentrations of Cu(II) ions were used. The system was maintained under shaking at 25 °C until adsorption equilibrium was reached. The adsorption capacities of Cu(II) ions were obtained from the initial, and the final concentration of Cu(II) ion in the solution determined by atomic adsorption spectrophotometer (WFX-ID) and the mass of adsorbent used.

Adsorption kinetics experiments were determined in a closed flask containing 0.10 g of *N*,*O*-CMC and 25.00 mL of copper sulfate solution (initial concentration 0.065 mol/L, pH 5.0) at 25 °C. During the kinetic experiments, aliquots samples were withdrawn at fixed time intervals, and the concentration of Cu(II) ions in solution was measured.

These batch experiments of the effects of pH, the temperature, the DS of *N*,*O*-CMC, and the ionic strength tests were carried out in the 25.00 mL of sulfate solution (initial concentration 0.065 mol/L, pH 5.0) shaking for 24 h at 25 °C, which

Table 1
Preparation conditions of *N*,*O*-CMC samples with different DS

Samples of *N*,*O*-CMC	Reaction conditions				
	Basification time (h)	Molar ratio of CTS to monochloroacetic acid	Method of addition	Reaction temperature (°C)	Reaction time (h)
DS = 0.72	12	1:1.25	Dropwise	70	2
DS = 0.88	12	1:1.25	Dropwise	60	8
DS = 0.96	12	1:1.25	Dropwise	60	4
DS = 1.06	12	1:1.25	Batch	60	2
DS = 1.15	12	1:1.25	Batch	60	3
DS = 1.25	12	1:1.25	Batch	60	4

were expected to provide information about the optimum conditions to adsorb with Cu(II) ions. The process of pH effect test was evaluated for Cu(II) ions in the range of pH 2.0–5.5 adjusted with 0.1 mol/L H_2SO_4 or ammonia/ammonium chloride.

2.5. Characterization

Fourier transform infrared spectra (FTIR) were obtained with a Perkin-Elmer FTIR 1600 series spectrometer and all samples were prepared as potassium bromide pellets.

X-ray photoelectron spectroscopy spectra of *N*,*O*-CMC with DS of 0.96 before and after copper(II) adsorption were recorded by using an X-ray Photoelectron Spectrometer (VG Scientific Escalab 210-UK) equipped with a twin anode (Mg Kα/Al Kα) source. The samples were placed in a vacuum in the range 10^{-8} to 10^{-7} Pa and the analyzed sample area was Ø6 mm–Ø6 μm. The scanning condition was as follows: 6.80 ms/step, 0.6 eV/step and 6 sweeps.

The micrographs of CTS and *N*,*O*-CMC with DS of 0.96 were taken using SEM (JSM-5600LV, JEOL Ltd.). Before SEM observation, samples of the composite were coated with gold.

3. Results and discussion

3.1. Characterization of N,O-CMC

3.1.1. IR analysis of N,O-CMC

The IR spectra of CTS and *N*,*O*-CMC with different DS are shown in Fig. 1. Fig. 1a shows the basic characteristics of CTS at: 3425 cm^{-1} (O–H stretching and N–H stretching), 2919 cm^{-1} (C–H stretching on methyl), 2879 cm^{-1} (C–H stretching in methylene), 1654 cm^{-1} (C=O of –NH–C=O stretching), 1596 cm^{-1} (N–H bending), 1085 and 1030 cm^{-1} (C–OH stretching). Comparing to Fig. 1a, the spectra of *N*,*O*-CMC show that a new absorption band near 1600 cm^{-1} attributed to C=O of –COONa stretching, and shift to high wavenumber in the IR spectrum of Fig. 1b–d with the increasing of the DS of *N*,*O*-CMC. Which indicates that the $-NH_2$ group of CMC was involved in the reaction. The bands corresponding

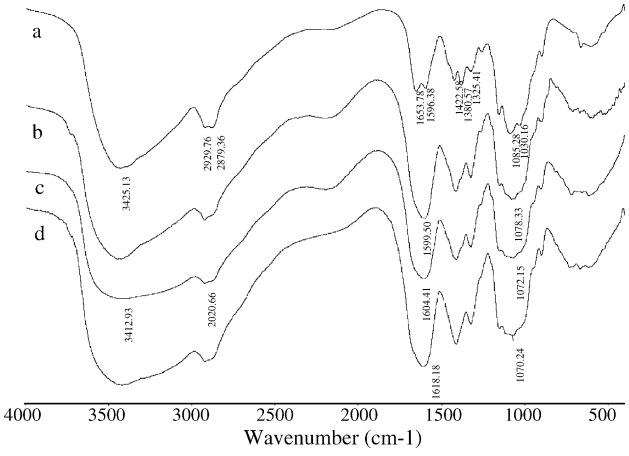

Fig. 1. IR spectra of CTS (a) and *N*,*O*-CMC with DS of 0.72 (b), 0.96 (c), 1.06 (d).

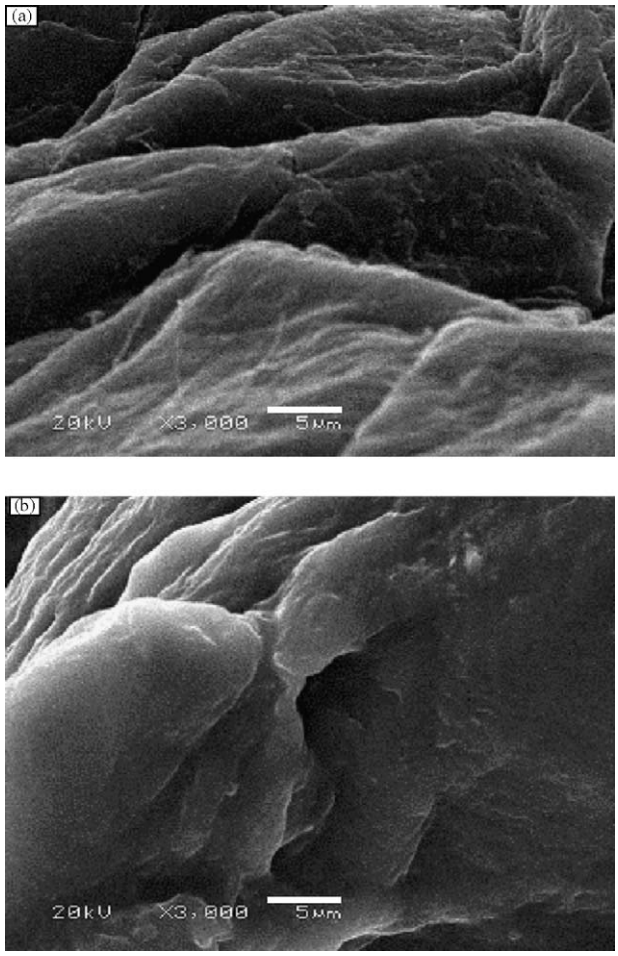

Fig. 2. SEM of CTS (a) and *N*,*O*-CMC with DS of 0.96 (b).

to the stretching vibration of the first and second –OH group weakened, which suggests that the –OH group of CMC with $-CH_2COOH$ take place the reaction. The intensity of the band at 3425 cm^{-1} of the stretching vibration of $-NH_2$ group and –OH group decreased with increase the DS of *N*,*O*-CMC. The IR analysis results of the derivatives show that the characteristic group (carboxyl group) exists in the product, and that $-CH_2COOH$ group has partly substituted the amino and hydroxyl of CTS.

3.1.2. SEM

The SEM observation of CTS and *N*,*O*-CMC is shown in Fig. 2. On the SEM of CTS (Fig. 2a), the surface is smooth and nonporous appears. While on the SEM of *N*,*O*-CMC (Fig. 2b), the surface is microporous. This result also indicated that CTS have been chemically modified.

3.2. Adsorption of N,O-CMC for Cu(II) ion

3.2.1. Adsorption isotherms

Generally, the adsorption capacity increases with the increase of the concentration of metal ions in the aqueous phase [21]. In the present work, the same adsorption phenomenon was observed when 0.005–0.09 mol/L of $CuSO_4$ was used. The result shown in Fig. 3 reveals that the *N*,*O*-CMC has a good adsorp-

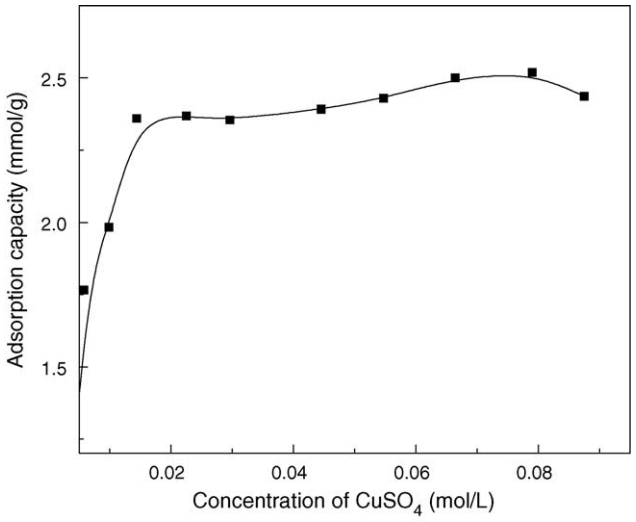

Fig. 3. Adsorption isotherm of *N*,*O*-CMC for Cu(II) ion.

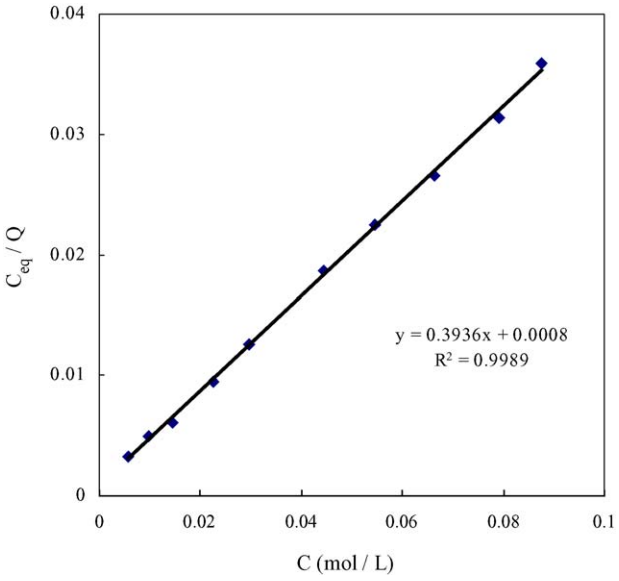

Fig. 4. Linearization of Langmuir adsorption isotherm.

tion capacity toward Cu(II). The sharp increase in capacity is observed from 0.005 to 0.02 mol/L, which is a four-fold increase in concentration, results in 34.1% increase in adsorption capacity, and when Cu(II) ion concentration increases from 0.02 to 0.08 mol/L, which is also a four-fold increase in concentration, results in only 4.3% increase in adsorption capacity. These results demonstrate that the formation of adsorption exists as physical adsorption and chemical adsorption. The adsorption is sensitive to the change under the low concentration of electrolyte, which shows that the adsorption is dominated by the electrostatic attraction (physical adsorption). Consequently, the electrostatic attraction does play a primary role in the complex formation between Cu(II) ions and *N*,*O*-CMC. In high concentration, the adsorption is insensitive to the change, and *N*,*O*-CMC displays an impressive ability to coordinate with Cu(II) ions and to yield the insoluble complexes, which indicates that the adsorption is dominated by the chelation. It can be seen that the high adsorption capacity of *N*,*O*-CMC with Cu(II) ion is in the range 0.06–0.08 mol/L.

From the analysis of isotherm, the value of the adsorption capacities, the concentration of Cu(II) ions, and the mathematical equation of isotherm were placed in a linear form more suitable for determination of adsorption parameters. The equation, which gave the best fit for the experimental isotherm data was the Langmuir model:

$$\frac{C}{Q} = \frac{C}{Q^0} + \frac{b}{Q^0} \quad (1)$$

where Q is the adsorption capacity at equilibrium, C the concentration of Cu(II) ions in the aqueous phase at equilibrium, Q^0 the saturation adsorption and b is the Langmuir constant.

The linearization of the equation is shown in Fig. 4. The linear curve obtained resulted in the following equation:

$$\frac{C}{Q} = 0.3936C + 0.0008 \quad (2)$$

This equation suggests that the Langmuir model is reasonable in interpreting the experimental data. The angular coefficient of this equation corresponds to the $1/Q^0$ and the intercept represents the $1/Q^0 b$. The value for the Q^0 was 2.54 mmol of Cu/g of *N*,*O*-CMC with DS of 0.96 (162.5 mg/g) and a Langmuir contant b of 2.03×10^{-3} g/mmol, which is same as the experimental data (2.52 mmol/g). This result was higher than that of CTS-HL obtained by Justi et al. (1.72 mmol/g) [21]. Chang and Chen reported that the maximum adsorption capacity for copper of Monodisperse chitosan-bound Fe_3O_4 nanoparticles was just 0.34 mmol/g [22]. In comparison of *N*,*O*-CMC, some of the previous studies [1,23,24] had shown that the maximum adsorption capacities for copper were lower. Therefore, the *N*,*O*-CMC improved the adsorption capacity for Cu(II) ions of the chemical modified CTS.

3.2.2. Adsorption kinetics

Fig. 5 shows the relationship between the adsorption time and adsorption capacities of *N*,*O*-CMC for copper ions. Within

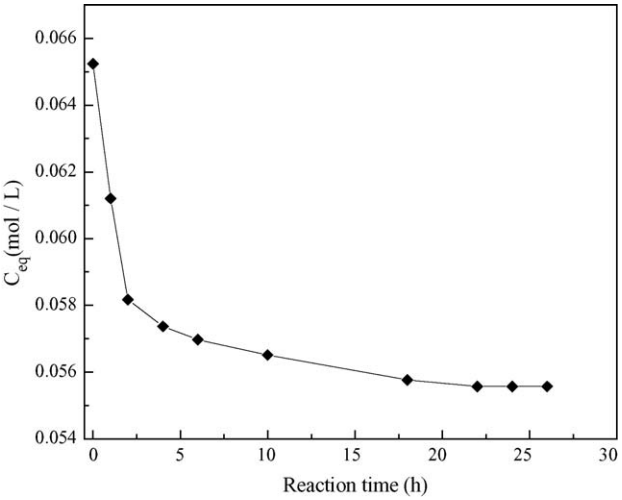

Fig. 5. Adsorption kinetics of *N*,*O*-CMC for Cu(II) ion.

5 h at 25 °C, the adsorption capacity increases rapidly at the early stage of the reaction, whereas from 5 to 22 h of reaction, a slight increase in the adsorption capacity is noted. Obviously, the adsorption capacity reaches equilibrium is observed beyond 22 h. As a result, the adsorption time of 22 h is optimal.

In order to evaluate the mechanism of the adsorption kinetics, the pseudo-first-order, pseudo-second-order and intraparticle diffusion models were tested to interpret the experimental data. The pseudo-first-order kinetic model of Chiou and Li [25] is given as:

$$\log(Q_{eq} - Q_t) = \frac{\log Q_{eq} - k_1 t}{2.303} \quad (3)$$

The pseudo-second-order equation [26] may be expressed as:

$$\frac{t}{Q_t} = \frac{1}{k_2 Q_{eq}{}^2} + \frac{t}{Q_{eq}} \quad (4)$$

The intraparticle diffusion rate [25] can be described as:

$$Q_t = k_i t^{1/2} \quad (5)$$

where Q_t is the adsorption capacity in time t (mmol/g), Q_{eq} the adsorption capacity at equilibrium (mmol/g) and k_1, k_2, k_i is the adsorption rate constant of pseudo-first-order (h^{-1}), pseudo-second-order (g/mmol/h), intraparticle diffusion rate (mmol/g/$h^{1/2}$), respectively. The validity of these models can be interpreted by the linear plots of $\log(Q_{eq}-Q_t)$ versus t, (t/Q_t) versus t and Q_t versus $t^{1/2}$, respectively [27].

As seen from Fig. 6 a–c, the correlation coefficients (R) given by the three kinetic models between the predicted and the experimental values are 0.8072, 0.9997, 0.8226, respectively. Obviously, the pseudo-second-order kinetic model, in contrast to the pseudo-first-order and intrarparticle diffusion models, gives a good correlation for the adsorption of Cu(II) ions on *N*,*O*-CMC.

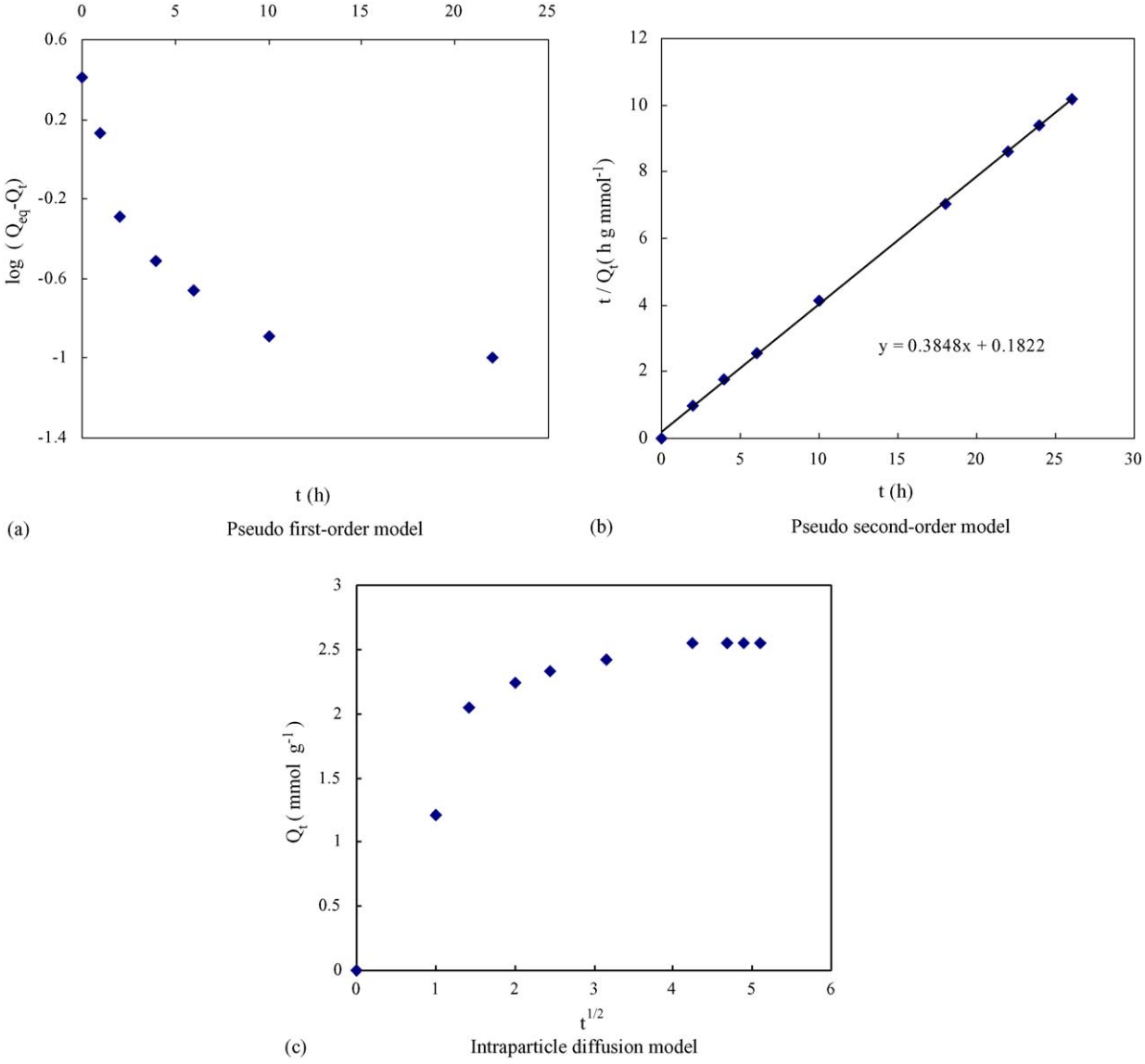

Fig. 6. Linearization of adsorption kinetics.

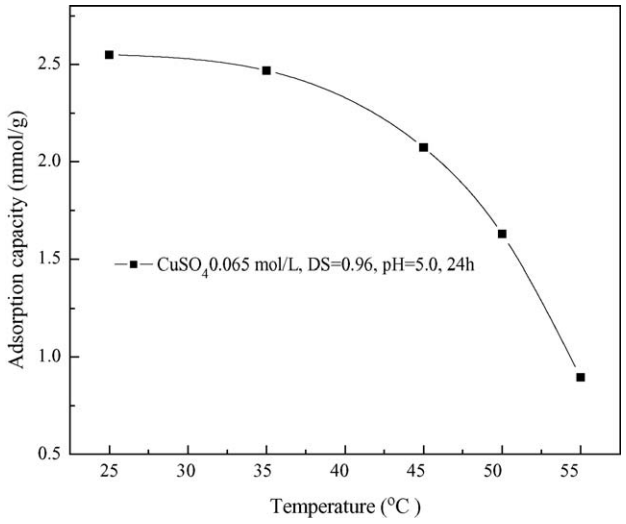

Fig. 7. Effect of reaction temperature on adsorption capacity of *N*,*O*-CMC for Cu(II) ion.

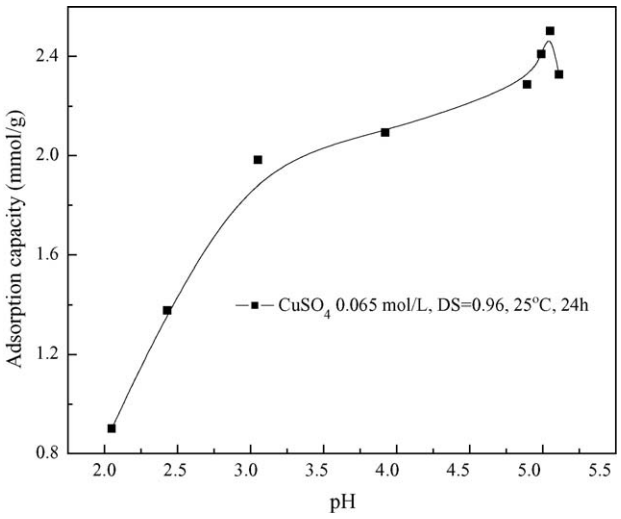

Fig. 8. Effect of pH on adsorption capacity of *N*,*O*-CMC for Cu(II) ion.

Kinetic studies on sorption of *N*,*O*-CMC for Cu(II) ions by using the pseudo-second-order rate expression provided the best fitting kinetic model. The mechanism indicates that the adsorption rate of Cu(II) ions depends on the concentration of ions at the adsorbent surface and the absorbance of these adsorbed at equilibrium. The rate constant k_2 determined is 0.8127 g/mmol/h.

3.2.3. Temperature effect

The influence of temperature on adsorption capacity of *N*,*O*-CMC for Cu(II) ions is shown in Fig. 7. The adsorption capacity of Cu(II) appears to decrease as the temperature is raised from 25 to 55 °C. It is found that the high temperature is to the disadvantage of adsorption and that the adsorption is an exothermic reaction. This result is distinct from the work of Lin et al. who pointed out that the adsorption of CMC for zinc ion was endothermic reaction [28]. Furthermore, it should be noted that excessively high temperature could result in solvent evaporation or some desorption, which affect the content of Cu(II) ions in solution.

3.2.4. Effect of pH value

Fig. 8 shows the relationship between the pH value in the original solution and the adsorption capacity of Cu(II) ions. As seen from Fig. 8, it is noteworthy that the adsorption capacity of Cu(II) ions increases with the pH of the solution until a maximum value of 5 and then decreases with an increase in pH value. At acidic pH, a decrease in the adsorption is attributed to the increase in ionic strength of solution and to the protonation of complexation sites. At alkaline pH, the Cu(II) ions in solution can form precipitate of copper hydroxide, which decreases the adsorption capacity.

3.2.5. Effect of DS of N,O-CMC

The reactions of equivalent $CuSO_4$ with *N*,*O*-CMC with different DS in the same conditions were conducted for determining the adsorption site. As seen from Fig. 9, the adsorption capacity increases with an increase of DS between 0.62 and 1.06. At the point of 1.06, a maximum value of adsorption capacity (2.73 mmol/g) is obtained. Between 1.06 and 1.25 the adsorption capacity decreases evidently. The non-linear phenomena lead us to conclude that the adsorption site of *N*,*O*-CMC was not only on $-COO^-$ but also on the other groups with different affinity, such as $-NH_2$ and $-OH$. These groups have interaction or synergistic action for Cu(II) adsorption.

3.2.6. Effect of ionic strength

Fig. 10 shows the relationship between the ionic strength and adsorption capacities of *N*,*O*-CMC for Cu(II) ions. The adsorption capacity decreases with increasing the amount of NaCl, which means that the adsorption reaction of *N*,*O*-CMC for Cu(II) was controlled by ionic strength. This is because of

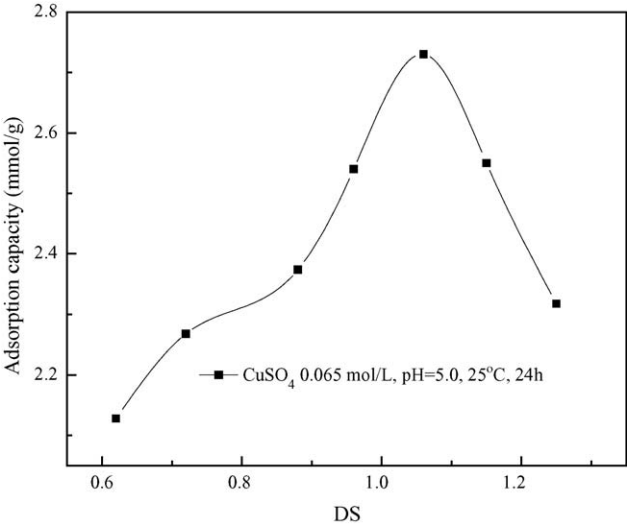

Fig. 9. Effect of DS on adsorption capacity of *N*,*O*-CMC for Cu(II) ion.

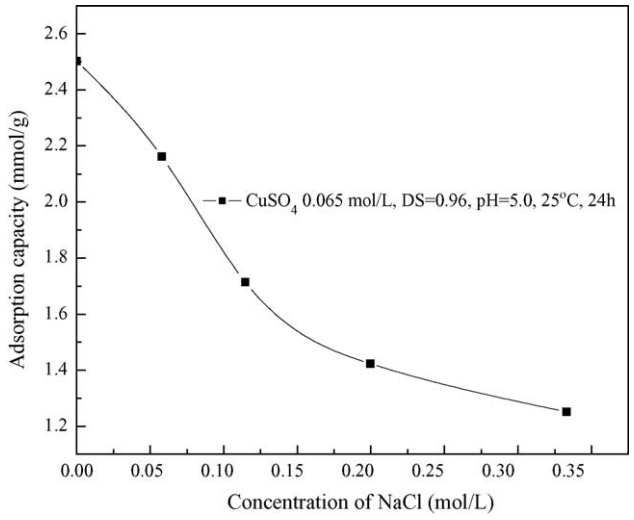

Fig. 10. Effect of ionic strength on adsorption capacity of *N*,*O*-CMC for Cu(II) ion.

two aspects. On the one hand, the affinity between *N*,*O*-CMC and metal ions declined with increasing the amount of NaCl, which causes the apparent adsorption velocity constant to decrease. On the other hand, the affinity between NaCl and H_2O (solvent) enhances with the addition of NaCl, which lead to the decrease of dielectric constant and ionic mobility. As a result, the interaction between solute and solvent in adsorption system and the adsorption rate decreases with the increasing the amount of NaCl.

3.3. Adsorption mechanism of Cu(II) ions

3.3.1. IR analysis

The spectrum of *N*,*O*-CMC after copper(II) adsorption (Fig. 11b) exhibits many alterations from that of *N*,*O*-CMC before copper(II) adsorption (Fig. 11a). The major differences are: the wide absorption band at 3419 cm^{-1}, corresponding to the stretching vibration of $-NH_2$ group and $-OH$ group, shifts to the lower wave number (3398 cm^{-1}). The absorption band

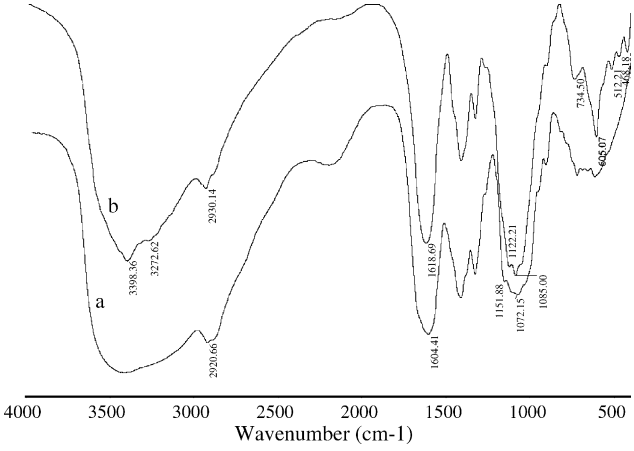

Fig. 11. IR spectra of *N*,*O*-CMC before (a) and after (b) copper(II) adsorption.

at 2920 cm^{-1}, assigned to C–H stretching vibration, shows a significant shift to higher wave number (2930 cm^{-1}). The absorption band at 1604 cm^{-1}, assigned to the stretching vibration of C=O of $-COO$-group, shifts to higher wave number (1619 cm^{-1}). Several new absorption bands are also observed in the spectrum of Fig. 11b. The bands at 1122 and 605 cm^{-1} are due to the stretching vibration of S–O band [29]. New bands are observed at 512 and 468 cm^{-1}, which are assigned to stretching vibration of N–Cu and O–Cu. This results indicates that the $-NH_2$, $-OH$ and $-COO^-$ group of *N*,*O*-CMC was involved in the adsorption process.

3.3.2. XPS

Fig. 12 shows the XPS spectra of C 1s, N 1s, O 1s, Cu $2p_{3/2}$ and S 2p of *N*,*O*-CMC before (Fig. 12a) and after (Fig. 12b) copper(II) ions adsorption. The relative intensities of the N 1s spectrum and the C 1s spectrum of Fig. 12b are evidently smaller than those of Fig. 12a, while the relative intensity of the O 1s spectrum is almost same with that of *N*, *O*-CMC before copper(II) adsorption. This is attributed to the adsorption of Cu(II) ions and plentiful oxygen contained in the copper sulfate, which lead to the decrease of the contents of nitrogen and carbon. At the same time, the new peaks of the Cu $2p_{3/2}$ and S 2p spectra are observed on *N*,*O*-CMC after copper(II) adsorption.

Table 2 shows the XPS spectra data of C 1s, O 1s, N 1s, Cu $2p_{3/2}$ and S 2p of *N*,*O*-CMC before (a) and after (b) copper(II) adsorption. Interestingly, the binding energy (BE) of C 1s is the same for *N*,*O*-CMC before and after copper(II) adsorption, while the BE of the C 1s decreases from 280.14 to 279.90 eV after absorbing Cu(II) ions by *N*,*O*-CMC. However, the BE of N 1s increases from 398.22 to 398.82 eV, while the BE of O 1s decreases from 531.50 to 531.38 eV, and the BE of Cu $2p_{3/2}$ shifts from 935.76 eV, that of $CuSO_4{\cdot}5H_2O$, to 932.46 eV, that of *N*, *O*-CMC after copper(II) adsorption. Evidently, nitrogen atom provides electron pair, and copper atom, oxygen atom and carbon atom are inclined to accept the electron. This implies that the $-NH_2$ group and $-COOH$ group are involved during the adsorption process. Furthermore, the BE of S 2p and O 1s decrease from 168.50, 532.50 to 168.20, 531.38 eV, respectively, which indicates that SO_4^{2-} exists not as free ion but as ion pair in the complex. From these results, electron transfer exists among the copper atom, sulfur atom, oxygen atom, carbon atom and nitrogen atom and the chemical bond formed among them, which provide evidence to the chelation between the *N*,*O*-CMC and Cu(II) ions during the adsorption process.

Table 2
XPS data of *N*,*O*-CMC before (a) and after (b) copper(II) adsorption

Sample	Binding energy (eV)					
	Cu $2p_{3/2}$	O 1s	N 1s	C 1s	C 1sa	S 2p
a	–	531.50	398.22	285.00	280.14	–
b	932.46	531.38	398.82	285.00	279.90	168.20
$CuSO_4{\cdot}5H_2O$	935.76	532.50	–	–	–	168.50

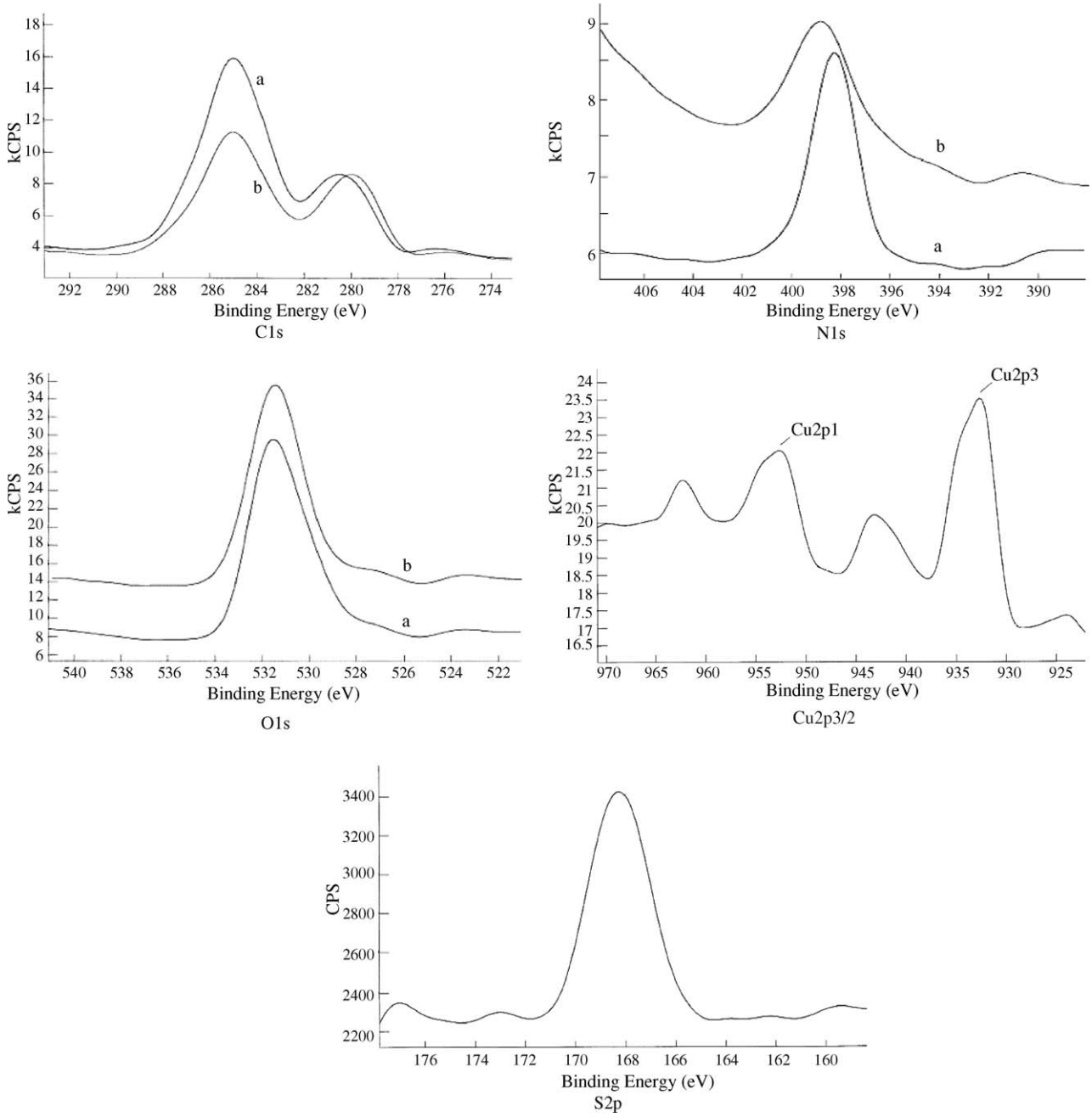

Fig. 12. XPS spectra of C 1s, N 1s, O 1s, Cu $2p_{3/2}$ and S 2p on *N*,*O*-CMC before (a) and after (b) copper(II) adsorption.

4. Conclusions

The characterization studies showed that the *N*,*O*-CMC was synthesized by CTS reaction with monochloroacetic. The results show that the Cu(II) ion adsorption process is dependent on pH, DS of *N*,*O*-CMC, temperature and ionic strength, and that the isotherm which best fits the adsorption data was the Langmuir monolayer model, and that the kinetics mechanism follows a pseudo-second-order model. FTIR and XPS studies revealed that Cu(II) ions coordinate to *N*,*O*-CMC and form the chelation complex. Furthermore, the maximum adsorption capacity of the monolayer for Cu(II) was 162.5 mg/g. Finally, this new material shows significant adsorption capacity for Cu(II) ion and can therefore be used as an alternative-adsorbing agent in static and dynamic separation processes.

References

[1] W.S. Wan Ngah, C.S. Endud, R. Mayanar, Removal of copper(II) ions from aqueous solution onto chitosan and cross-linked chitosan beads, React. Funct. Polym. 50 (2002) 181–190.
[2] R.S. Juang, H.J. Shao, A simplified equilibrium model for sorption of heavy metal ions from aqueous solutions on chitosan, Water Res. 36 (12) (2002) 2999–3008.
[3] C.P. Huang, Y.C. Chung, M.R. Liou, Adsorption of Cu(II) and Ni(II) by pelletized biopolymer, J. Hazard. Mater. 45 (1996) 265–277.

[4] F.C. Wu, R.L. Tseng, R.S. Juang, Comparative adsorption of metal and dye on flake- and bead-types of chitosans prepared from fishery wastes, J. Hazard. Mater. B 73 (2000) 63–75.
[5] K.H. Chu, Removal of copper from aqueous solution by chitosan in prawn shell: adsorption equilibrium and kinetics, J. Hazard. Mater. B90 (2002) 77–95.
[6] J.R. Evans, W.G. Davids, J.D. MacRae, A. Amirbahman, Kinetics of cadmium uptake by chitosan-based crab shells, Water Res. 36 (13) (2002) 3219–3226.
[7] E. Guibal, Interactions of metal ions with chitosan-based sorbents: a review, Sep. Purif. Technol. 38 (2004) 43–74.
[8] S.T. Lee, F.L. Mi, Y.J. Shen, S.S. Shyu, Equilibrium and kinetic studies of copper (II) ion uptake by chitosan-tripolyphosphate chelating resin, Polymer 42 (2001) 1879–1892.
[9] C.A. Rodrigues, M.C. Laranjeira, V.T. Favere, E. Stadler, Interaction of Cu(II) on *N*-(2-pyridylmethyl) and *N*-(4-pyridylmethyl) chitosan, Polymer 39 (1998) 5121–5126.
[10] K. Inoue, K. Yoshizuka, K. Ohto, Adsorptive separation of some metal ions by complexing agent types of chemically modified chitosan, Anal. Chim. Acta 388 (1999) 209–218.
[11] Z. Jia, D. Shen, W. Xu, Synthesis and antibacterial activities of quaternary ammonium salt of chitosan, Carbohydr. Res. 333 (2001) 1–6.
[12] Z.P. Zhao, Z. Wang, N. Ye, S.C. Wang, A novel *N*,*O*-carboxymethyl amphoteric chitosan/poly (ethersulfone) composite MF membrane and its charged characteristics, Desalination 144 (2002) 35–39.
[13] X.F. Liu, Y.L. Guan, D.Z. Yang, Z. Li, K.D. Yao, Antibacterial action of chitosan and carboxymethylated chitosan, J. Appl. Polym. Sci. 79 (2001) 1324–1335.
[14] N.S. Hon, L.G. Tang, Chelation of chitosan derivatives with zinc ions. I. *O*,*N*-carboxymethyl chitosan, J. Appl. Polym. Sci. 77 (2000) 2246–2253.
[15] R.A.A. Muzzarelli, P.I. Petrarulo, Solubility and structure of *N*-carboxymethyl chitosan, Int. J. Biol. Macromol. 16 (1994) 177–180.
[16] L. Zhang, J. Guo, J. Zhou, G. Yang, Y.M. Du, Blend membranes from carboxymethylated chitosan/alginate in aqueous solution, J. Appl. Polym. Sci. 77 (2000) 610–616.
[17] Y. Nuhoglu, E. Oguz, Removal of copper(II) from aqueous solutions by biosorption on the cone biomass of *Thuja orientalis*, Process. Biochem. 38 (2003) 1627–1631.
[18] X.G. Chen, H.J. Park, Chemical characteristics of *O*-carboxymethyl chitosans related to the preparation conditions, Carbohydr. Polym. 53 (2003) 355–359.
[19] C.X. Liu, G.H. Chen, Z.T. Jin, M.K. Sun, C.J. Gao, Modification of the formula for calculation of substitution degree of *N*,*O*-carboxymethyl chitosan, J. Beijing Univ. Chem. Technol. 31 (2004) 14–17 (in Chinese).
[20] S.J. Lu, X. Song, D. Cao, Preparation of water-soluble chitosan, J. Appl. Polym. Sci. 91 (2004) 3497–3503.
[21] K.C. Justi, M.C.M. Laranjeira, A. Neves, Chitosan functionalized with 2-bis-(pyridylmethyl) aminomethyl-4-methyl-6-formyl-phenol: equilibrium and kinetics of copper(II) adsorption, Polymer 45 (2004) 6285–6290.
[22] Y.C. Chang, D.H. Chen, Preparation and adsorption properties of monodisperse chitosan-bound Fe_3O_4 magnetic nanoparticles for removal of Cu(II) ions, J. Colloids Interf. Sci. 283 (2005) 446–451.
[23] M.M. Beppu, E.J. Arruda, R.S. Vieira, N.N. Santos, Adsorption of Cu(II) on porous chitosan membranes functionalized with histidine, J. Membr. Sci. 240 (2004) 227–235.
[24] T. Mitani, T. Kawakami, M. Morishita, Y. Adachi, H. Ishii, Effect of copper adsorption on the mechanical properties of chitosan beads, J. Appl. Polym. Sci. 88 (2003) 2988–2991.
[25] M.S. Chiou, H.Y. Li, Adsorption behaviour of reactive dye in aqueous solution on chemical cross-linked chitosan beads, Chemosphere 50 (2003) 1095–1105.
[26] W.S.W. Ngah, S. Ab Ghani, A. Kamari, Adsorption behaviour of Fe(II) and Fe(III) ions in aqueous solution on chitosan and cross-linked chitosan beads, Bioresour. Technol. 96 (2005) 443–450.
[27] F.C. Wu, R.L. Tseng, R.S. Juang, Kinetic modeling of liquid-phase adsorption of reactive dyes and metal ions on chitosan, Water Res. 35 (3) (2001) 613–618.
[28] Y.W. Lin, W. Chen, H.B. Luo, Z. Jiang, Study on the adsorption of Zn(II) in solution by carboxymethyl chitosan, Strait Pharmaceut. J. 12 (3) (2000) 69–72 (in Chinese).
[29] X.H. Wang, Y.M. Du, H. Liu, Preparation, characterization and antimicrobial activity of chitosan–Zn complex, Carbohydr. Polym. 56 (2004) 21–26.